MDPI

Article

Magnetic Field Gradient-Based EKF for Velocity Estimation in Indoor Navigation

Makia Zmitri [1], Hassen Fourati [1]* and Christophe Prieur [1]

[1] Univ. Grenoble Alpes, CNRS, Grenoble INP, GIPSA-lab, F-38000 Grenoble, France;
* Correspondence: hassen.fourati@gipsa-lab.fr.

Version July 24, 2020 submitted to Sensors

Abstract: This paper proposes an advanced solution to improve the inertial velocity estimation of a rigid body, for indoor navigation, through implementing a magnetic field gradient-based Extended Kalman Filter (EKF). The proposed estimation scheme considers a set of data from a triad of inertial sensors (accelerometer and gyroscope), as well as a determined arrangement of magnetometers array. The inputs for the estimation scheme are the spatial derivatives of the magnetic field, from the magnetometers array, and the attitude, from the inertial sensors. As it was shown in the literature, there is a strong relation between the velocity and the measured magnetic field gradient. However, the latter usually suffers from high noises. Then, the novelty of the proposed EKF is to develop a specific equation to describe the dynamics of the magnetic field gradient. This contribution helps to filter, first, the magnetic field and its gradient and second, to better estimate the inertial velocity. Some numerical simulations that are based on an open source database show the targeted improvements. At the end of the paper, this approach is extended to position estimation in the case of a foot-mounted application and the results are very promising.

Keywords: Indoor navigation; magnetic field gradient; spatial derivatives; inertial velocity estimation; Extended Kalman Filter.

1. Introduction

Nowadays, the interest in indoor positioning has been growing exponentially, as it represents a topic of research for many different applications, such as health [1], [2], sports [3], military [4], etc. A wide range of techniques has been investigated to tackle this problem. Some of them require a costly, heavy and pre-installed infrastructure to work (e.g. Wireless Local Area Network (WLAN) [5], Radio Frequency Identification (RFID) [6], etc.). Others rely on more traditional methods such as computer vision techniques [7], which can be inaccessible in certain situations (smoke in building for instance). The most common solution to the case where the conditions of intervention, and the availability of pre-installed equipment are unknown, is the use of low-cost Inertial Measurement Units (IMUs), composed of inertial and magnetic sensors. It represents a promising key to solve many problems in indoor positioning. Usually, the outputs of IMUs are used to calculate the velocity and position through an integration process, or to determine the orientation (attitude) [8] through a specific fusion. Nevertheless, because of sensors biases and noises, these integrations are biased, and then a drift is observed on velocity (integration of linear acceleration) and position (integration of velocity). Numerous techniques have been proposed in the literature to deal with this problem. Some of them depend on a foot-mounted dead reckoning method called Zero-Velocity Update Technique (ZUPT), like in [9] and [10], for example. This method allows to reduce the integration to small steps between phases where the foot is at rest on the ground (stance phase). The drift on velocity and position is thus reduced, especially for the accelerometer measurements integration, which allows a longer use before the system diverges too far away from the actual position. In that process, the better is the velocity,

the better is its integration to obtain an improved position. The inertial velocity is also important in other applications, that are not necessarily related to the position estimation. For instance, in [11], drifts in attitude estimation for human and animal motion evaluation are corrected by removing transient accelerations, using a mathematical derivation of velocity measurements coming from a Global Positioning System (GPS) receiver. In the case where GPS measurements are unavailable, or inaccurate, the precision of this proposed approach is degraded. In [12], it is discussed that velocity sensors attached to swimming animals are potentially inaccurate. An evaluation is then conducted with an ellipsoidal micro-turbine that is used to measure the through water speed of a dolphin, by being attached to its body using an array of suction cups. The obtained speed measurements suffer from few drawbacks, such as the inability to track the speed of the disturbed flow when it drops below the turbine stall speed ($U \approx 0.25 m/s$). Other works used the velocity, obtained from a GPS receiver only in the case of outdoor navigation, as an important feature for the classification and prediction of transportation modes [13], [14].

1.1. Context

The main problem under investigation is the velocity estimation in indoor navigation by means of inertial and magnetic sensors. As known, the presence of magnetic perturbations in indoor environments can be very large [15], due to all metals used in buildings (door frames, aluminum windows, etc.) and potentially to the strong electric currents propagating close-by. Now, one might think that these disturbances can only represent a constraint for indoor positioning. However, these perturbations are not in fact a random noise. On the contrary, they are well structured by physics equations, for instance, Maxwell's equations [16]. The latter represent the propagation of electromagnetic phenomena. Therefore, it is considered that rich information lies in these disturbances. In [17], authors use measurements from an array of 3-axis magnetometers to derive a maximum likelihood estimator. This is in order to determine the displacement of a body through a spatially varying magnetic field. Another recent approach that requires the use of only a 3-axis magnetometer's array, a 3-axis accelerometer and a 3-axis gyroscope, has been firstly introduced in [18], [19]. The proposed technique takes advantage of the magnetic field disturbances, that are observed indoors, to estimate the inertial velocity. This preserves the main advantages of purely inertial technology: no prior mapping or other information are required. Based on this idea, but with different dynamic models, other authors have shown in [20], [21], efficient velocity and position estimation results. In fact, they proved that as long as the magnetic field gradient is non-singular, the velocity is observable and there exists a converging non-linear observer that reconstructs it. In these works, the magnetic field gradient is considered as a measured input for the state-space model and the observer. However, this gradient is usually noisy and is subject to singularities. This influences negatively the observability of the proposed models, which leads to estimation errors. Contrarily, in [19], the authors considered that the magnetic field gradient is not available, instead, the gradient is moved to the state vector and is estimated by an observer. Nevertheless, the gradient's dynamics are modeled by a white noise, which is a questionable choice to the best of authors knowledge, and can influence the estimation of velocity.

1.2. Contribution

This paper presents a solution to improve the inertial velocity estimation. The proposed approach takes advantage of magnetic disturbances, by using a set of spatially distributed magnetometers to monitor the magnetic field and its spatial derivatives (gradient and its first derivative). The considered state-space model in this work also includes a new magnetic field gradient equation, derived to describe its dynamic. An EKF is proposed to better estimate the inertial velocity in a magnetically disturbed environment, from a 3-axis magnetometer's array, a 3-axis gyroscope and a 3-axis accelerometer. The novelty in the proposed approach is the development of this specific equation to describe the dynamics of magnetic field gradient. This contribution helps better filter the magnetic field and its gradient.

Moreover, it improves the estimation of inertial velocity. The inputs for the estimation scheme are the spatial derivatives of the magnetic field, from the magnetometer's array, and a determined attitude via a gradient descent algorithm, from a triad of inertial and magnetic sensors. A notable improvement on the velocity estimation is shown compared to when the noisy magnetic field gradient is measured and used as an input for the EKF. At the end of the paper, we examine the effect of such velocity improvement on the position estimation in the case of a foot-mounted application aided by ZUPT and the results are very promising.
This paper is organized as follows. In Section 2 some preliminaries and notations are introduced and the principle of magneto-inertial navigation problem is stated, then the magnetic field gradient dynamic equation is established. An EKF is designed in Section 3, where the gradient equation is added, to tackle measurement noises and to estimate not only the velocity but also the magnetic field and its gradient. The EKF is fed with a determined quaternion, given by an attitude estimation block. In Section 4, the ZUPT-aided position estimation is detailed, based on the previous velocity estimation, in the context of foot-mounted inertial navigation. Section 5 presents a scenario test based on an open source database [22] representing a foot-mounted navigation scheme. The obtained results in this case are displayed. While in Section 6, some conclusions and potential future works are stated.

2. Problem formulation

The problem under consideration is how to improve the inertial velocity estimation using only Micro Electro Mechanical Systems (MEMS) inertial sensors, composed of a 3-axis accelerometer and a 3-axis gyroscope, as well as a spatially distributed 3-axis magnetometer's array. A new state-space model is proposed and its contribution is demonstrated through an EKF-based approach. In the end of the paper, the obtained results of the improved velocity estimation are extended to the position estimation in a foot-mounted framework.

2.1. Notation

To address the problem cited above, two frames are used:

- a local inertial frame $\Re_n$ fixed to the Earth and its associated orthonormal basis $\mathfrak{B}_\mathfrak{n} = (\vec{i}_n, \vec{j}_n, \vec{k}_n)$;
- a body frame $\Re_b$ attached to the moving rigid body and its associated orthonormal basis $\mathfrak{B}_\mathfrak{b} = (\vec{i}_b, \vec{j}_b, \vec{k}_b)$.

Variables expressed in $\Re_n$ (resp. $\Re_b$) are marked by the subscript n (resp. b).
Let $R_{b\leftarrow n} \in SO(3)$ be the rotation matrix between the two frames, from $\Re_n$ to $\Re_b$. For the sake of simplicity, in the rest of the paper the notation $R_{b\leftarrow n}$ is omitted and is replaced by R. This matrix can be expressed in terms of quaternion as follows

$$R = \begin{bmatrix} 2(q_0^2+q_1^2)-1 & 2(q_1q_2+q_0q_3) & 2(q_1q_3-q_0q_2) \\ 2(q_1q_2-q_0q_3) & 2(q_0^2+q_2^2)-1 & 2(q_0q_1+q_2q_3) \\ 2(q_0q_2+q_1q_3) & 2(q_2q_3-q_0q_1) & 2(q_0^2+q_3^2)-1 \end{bmatrix} \tag{1}$$

The unit quaternion, denoted by q, is a hypercomplex number of rank 4 such that,

$$q = [q_0 \quad q_{vect}^\top]^\top \tag{2}$$

where q_0 is the scalar part and $q_{vect} = [q_1 \quad q_2 \quad q_3]^\top$ is the vector part of quaternion. The reader is invited to refer to [23] for more details about quaternion algebra.
The rigid body under consideration can simultaneously translate and rotate in 3D space, and its displacement is represented with the position vector $M_n = [x_n \quad y_n \quad z_n]^\top \in \mathbb{R}^{3\times1}$ in $\Re_n$. Then $v_n = \frac{dM_n}{dt} = [v_{nx} \quad v_{ny} \quad v_{nz}]^\top \in \mathbb{R}^{3\times1}$ the inertial velocity vector, to be estimated in $\Re_n$, and $a_n = \frac{dv_n}{dt} = [a_{nx} \quad a_{ny} \quad a_{nz}]^\top \in \mathbb{R}^{3\times1}$ the acceleration vector. Vectors v_n and a_n can also be expressed in $\Re_b$ by simply multiplying them by R.

Since inertial and magnetic sensors are used in this framework, then the following variables are considered:

- The angular velocity $\omega^{\frac{b}{n}} = [\omega_x \ \ \omega_y \ \ \omega_z]^\top \in \mathbb{R}^{3\times 1}$, of $\Re_b$ with respect to $\Re_n$, measured by a 3-axis gyroscope. The corresponding skew-symmetric matrix is defined such as

$$[\omega^{\frac{b}{n}}\times] = \begin{pmatrix} 0 & -\omega_z & \omega_y \\ \omega_z & 0 & -\omega_x \\ -\omega_y & \omega_x & 0 \end{pmatrix} \tag{3}$$

- The acceleration $a_b = [a_{bx} \ \ a_{by} \ \ a_{bz}]^\top \in \mathbb{R}^{3\times 1}$ of $\Re_b$, measured by a 3-axis accelerometer;
- The magnetic field $B_b = [B_{bx} \ \ B_{by} \ \ B_{bz}]^\top \in \mathbb{R}^{3\times 1}$, measured in $\Re_b$ by a 3-axis magnetometer, which depends on time and space;
- The Jacobian matrix $\nabla B_b \in \mathbb{R}^{3\times 3}$, which represents the magnetic field gradient, measured on a fixed point $P_b = [x_{bp} \ \ y_{bp} \ \ z_{bp}]^\top \in \mathbb{R}^{3\times 1}$ and defined by

$$\nabla B_b(P_b(t)) = \frac{\partial B_b(P_b(t))}{\partial P_b(t)} \tag{4}$$

2.2. Magnetic field and its gradient

A rigid body located inside a magnetically disturbed area is considered, which is a situation that is often observed indoors [15]. The disturbances on the magnetic field are useful information in this work. According to Maxwell's equations [16], the dynamic of the magnetic field measured in $\Re_b$ obeys to the following equation[1]

$$\frac{dB_b}{dt} = -\omega^{\frac{b}{n}} \times B_b + \nabla B_b v_b \tag{5}$$

This equation ensures that v_b is observable and can be estimated, provided that ∇B_b is non-singular (see [18] for observability proof). Under this assumption, the velocity can be estimated using ∇B_b, which enhances the performance of any inertial navigation system, as it has been demonstrated in [19]. However, one of the major remaining difficulties, is to reliably measure ∇B_b. For this purpose, a spatially distributed magnetometer's array is considered. This array provides magnetic field measurements that are usually noisy, then, when computing spatial derivatives, this noise can get larger. It follows that ∇B_b is also corrupted by noise. This noise can degrade the velocity estimation especially when ∇B_b has low values (more precise simulations on the matter are in [20]). A way to tackle this problem is to filter ∇B_b. To do so, an equation representing its dynamic should be proposed. For that, the temporal derivative of ∇B_n in $\Re_n$ is introduced such as,

$$\frac{d\nabla B_n}{dt} = \frac{d\nabla B_n}{dM_n}\frac{dM_n}{dt} = T_n v_n \tag{6}$$

where $T_n \in \mathbb{R}^{3\times 3\times 3}$ is a tensor representing the first spatial derivative of ∇B_n in $\Re_n$ and can be represented as follows:

$$T_n = \frac{d\nabla B_n}{dM_n} = \begin{bmatrix} \nabla\alpha_{11} & \nabla\alpha_{12} & \nabla\alpha_{13} \\ \nabla\alpha_{21} & \nabla\alpha_{22} & \nabla\alpha_{23} \\ \nabla\alpha_{31} & \nabla\alpha_{32} & \nabla\alpha_{33} \end{bmatrix} \tag{7}$$

and $\nabla\alpha_{ij} = [\frac{\partial\alpha_{ij}}{\partial x_m} \ \ \frac{\partial\alpha_{ij}}{\partial y_m} \ \ \frac{\partial\alpha_{ij}}{\partial z_m}]_{1\leq i,j\leq 3}$, with α_{ij} representing the elements of ∇B_n.

---

[1] $\times$ is the cross product of two vectors in $\mathbb{R}^3$.

The temporal derivative $\frac{d\nabla B_n}{dt}$ can also be written such as

$$\frac{d\nabla B_n}{dt} = \frac{d(R^\top \nabla B_b R)}{dt} = \frac{dR^\top}{dt}\nabla B_b R + R^\top \frac{d\nabla B_b}{dt} R + R^\top \nabla B_b \frac{dR}{dt}$$
$$= R^\top [\omega^{\frac{b}{n}}\times]\nabla B_b R + R^\top \frac{d\nabla B_b}{dt} R + R^\top \nabla B_b (-[\omega^{\frac{b}{n}}\times]R) \quad (8)$$

From (6) and (8) the following equality is obtained

$$R^\top \frac{d\nabla B_b}{dt} R = T_n v_n + R^\top \nabla B_b [\omega^{\frac{b}{n}}\times]R - R^\top [\omega^{\frac{b}{n}}\times]\nabla B_b R \quad (9)$$

By multiplying both sides of (9) by R and $R^\top$ respectively, the following equation is deduced,

$$\frac{d\nabla B_b}{dt} = T_b v_b + \nabla B_b [\omega^{\frac{b}{n}}\times] - [\omega^{\frac{b}{n}}\times]\nabla B_b \quad (10)$$

where T_b is the first spatial derivative of ∇B_b, with the same form as (7), represented in $\Re_b$. The reader can check [24] for more information on how T_b is measured.
In Section 3, the dynamic model, specific to the studied problem, is expanded by including (10), and an EKF is designed to filter ∇B_b to improve the velocity estimation.

3. Inertial velocity, magnetic field and magnetic field gradient estimation

This section is focused mainly on the inertial velocity estimation, by using an IMU and an array of spatially distributed magnetometers. A block diagram of the proposed approach is shown in Fig. 1. The main novelty resides on the blue block, which represents a magnetic field gradient-based EKF for estimating not only the inertial velocity $\widehat{v_n}$, but also the magnetic field $\widehat{B_b}$, and its gradient $\widehat{\nabla B_b}$. This EKF is fed with an estimated quaternion $\widehat{q}$, given by the green block, that depicts a gradient descent attitude estimation algorithm [25]. The two blocks are explained in details in the following sub-sections.

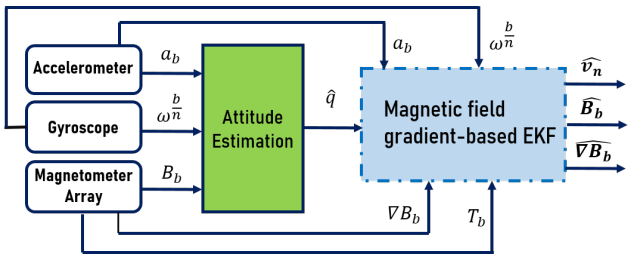

Figure 1. Overall diagram for estimation

3.1. Magnetic field gradient-based EKF

A magnetic field gradient-based EKF is proposed based on a 3-axis magnetometer's array, a 3-axis gyroscope and a 3-axis accelerometer. The continuous-time dynamic model used to establish the EKF can be written such as

$$\begin{cases} \frac{dv_n}{dt} = R(\widehat{q})^\top a_b - g \\ \frac{dB_b}{dt} = -\omega^{\frac{b}{n}} \times B_b + \nabla B_b R(\widehat{q}) v_n \\ \frac{d\nabla B_b}{dt} = T_b R(\widehat{q}) v_n + \nabla B_b [\omega^{\frac{b}{n}}\times] - [\omega^{\frac{b}{n}}\times]\nabla B_b \end{cases} \quad (11)$$

The state vector for this dynamic state-space model is $x = [v_n \;\; B_b \;\; \nabla B_b]^\top \in \mathbb{R}^{11\times 1}$, the input vector is $u = [\widehat{q} \;\; \omega_{nb}^{b} \;\; a_b \;\; T_b]^\top \in \mathbb{R}^{17\times 1}$, and the output (measurement) vector is $y = [B_b \;\; \nabla B_b]^\top \in \mathbb{R}^{8\times 1}$. Recall that 7 elements of T_b are sufficient to calculate all the tensor's components [24]. The matrix $R(\widehat{q})$ is defined in (1), where $\widehat{q}$ is the estimated quaternion. Note that the term v_b in (5) and (10) is replaced by $R(\widehat{q})v_n$ since the inertial velocity needs to be estimated in $\Re_n$ rather than in $\Re_b$.
The magnetic field measurements are usually noisy, then, when extracting higher order derivatives (in this case ∇B_b), this noise can get more important, due to the different approximations taken into account in some numerical computations. It follows that ∇B_b is also affected by noise. This can cause unbounded velocity estimation errors especially when ∇B_b has low values (more precise simulations on the matter are in [20]). For this reason, filtering ∇B_b instead of using it directly as an input, corrupted with noise, in the EKF, improves the velocity estimation. As T_b, defined in (10), is measurable, it is possible to add ∇B_b to x. A first schema of the magnetic field gradient-based EKF was presented in [24]. The estimation approach was based on two EKFs, in cascade, as displayed in Fig. 2. The primary EKF used the third equation in (11) as a dynamic model while the main EKF used the first and second equations in (11).

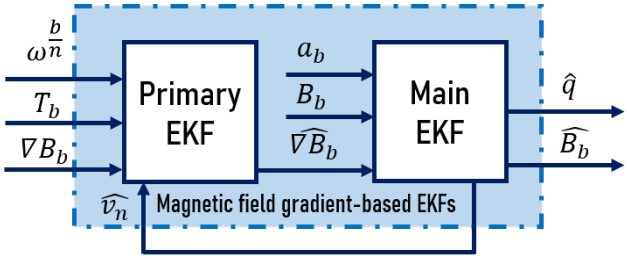

Figure 2. Magnetic field gradient-based EKFs [24]

To go further in this paper, we propose to simplify the estimation architecture in Fig. 2, by using the compact dynamic model (11). The general schema of estimation is presented in Fig. 3, where a single EKF is rather used.

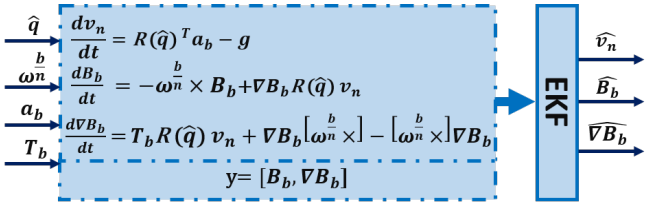

Figure 3. Magnetic field gradient-based EKF

The two models for process and measurements in Fig. 3 can be represented by the following general nonlinear form:

$$\begin{aligned} x[k] &= f(x[k-1], u[k], v[k]) \\ y[k] &= h(x[k], u[k], \eta[k]) \end{aligned} \tag{12}$$

where $x[k]$ is the state vector at time step k, $y[k]$ is the measurement vector, $u[k]$ is the input, $f(.)$ is a nonlinear function that represents the state-space model, $h(.)$ is a nonlinear function that represents the measurement model, and $v[k]$ and $\eta[k]$ are the process and measurement noises, respectively, and are assumed to be zero-mean, white, Gaussian and uncorrelated. Note that in order to determine $f(.)$ and $h(.)$, a discretization procedure that transforms the continuous-time equations in Fig. 3 into a discrete-time model must be undertaken. The Runge-Kutta 4^{th} order method [26] is used for the discretization.

3.2. Quaternion estimation

The kinematic equation describing the variation of rigid body's attitude in term of quaternion, can be defined from angular velocity measurements given by a 3-axis gyroscope such as,

$$\frac{dq}{dt} = \frac{1}{2}[\omega_q \times]q = \frac{1}{2}\begin{pmatrix} 0 & -\omega_x & -\omega_y & -\omega_z \\ \omega_x & 0 & \omega_z & -\omega_y \\ \omega_y & -\omega_z & 0 & \omega_x \\ \omega_z & \omega_y & -\omega_x & 0 \end{pmatrix} q \tag{13}$$

where $\omega_q = [0 \quad \omega^{\frac{b}{n}\top}]^\top \in \mathbb{R}^{4\times 1}$, the quaternion form of angular velocity, and $[\omega_q \times]$ is its skew-symmetric matrix. However, the gyroscope has a long-term drift which is due to noise and bias. So, by simply integrating (13), a drift can be observed on quaternion. The most common solution for such problem is to use a data fusion approach that merges measurements coming from gyroscopes, accelerometers, and magnetometers. The main methods are based on Kalman filters (KFs) [27], Extended Kalman filters (EKFs) [28], complementary filters [29], [25], [30], or observers [31]. Nevertheless, one should keep in mind the problem of magnetic disturbances in indoor navigation. These perturbations are known to affect the precision of most attitude determination techniques, which calls for approaches that investigate this case, such as in [28], [31] and [25].
In [25], authors proposed a new algorithm that uses inertial and magnetic measurements to provide a precise attitude estimation through incorporating magnetic distortion and gyroscope drift compensations. The main idea is to use a 3-axis accelerometer and a 3-axis magnetometer measurements in an analytically derived and optimized gradient descent algorithm, in order to compute the direction of gyroscope measurement error as a quaternion derivative. This algorithm is computationally inexpensive, as it requires 277 scalar arithmetic operations each update step, it is efficient at low sampling rates and it has only two adjustable parameters defined by observable system characteristics. Moreover, it eliminates the need for the reference direction of Earth's magnetic field to be predefined. Then, in what follows, this algorithm is implemented (green block in Fig. 1) to determine $\widehat{q}$.

4. Position estimation in the context of foot-mounted inertial navigation

In this section, we examine the effect of such velocity estimation improvement on the position one, with a focus on a foot-mounted navigation framework. The proposed algorithm is a combination between the magnetic field gradient-based EKF and ZUPT. The general schema of estimation is presented in Fig. 4. The right red block represents the zero-velocity detector, denoted d. In the case where $d = 1$, a zero-velocity update (left red block) is applied on the estimated inertial velocity $\widehat{v_n}$ resulting from the blue block. The updated velocity $\widehat{v_{nZupt}}$ is fed to the yellow block for integration, in order to obtain the position $\widehat{M_n}$. The red blocks are described in the following subsections.

4.1. Zero-velocity detector

The objective of a zero-velocity detector is to decide whether, during a time epoch that consists of $W \in \mathbb{N}$ observations (i.e. window size) between the time instants l and $l + W - 1$, the IMU is moving or stationary, given the measurements a_b and $\omega^{\frac{b}{n}}$. At each sample, this detector, denoted d, can have one of the two values: $d = 1$, which corresponds to the stance phase (the entire period during which the foot is on the ground) or $d = 0$, which represents the swing phase (the entire period during which the foot is in the air for limb advancement). Mathematically, this detection process can be seen as a binary hypothesis testing problem, where the detector indicates that the IMU is stationary (i.e. $d = 1$) if,

$$T_s(a_b, \omega^{\frac{b}{n}}) \leq \gamma \tag{14}$$

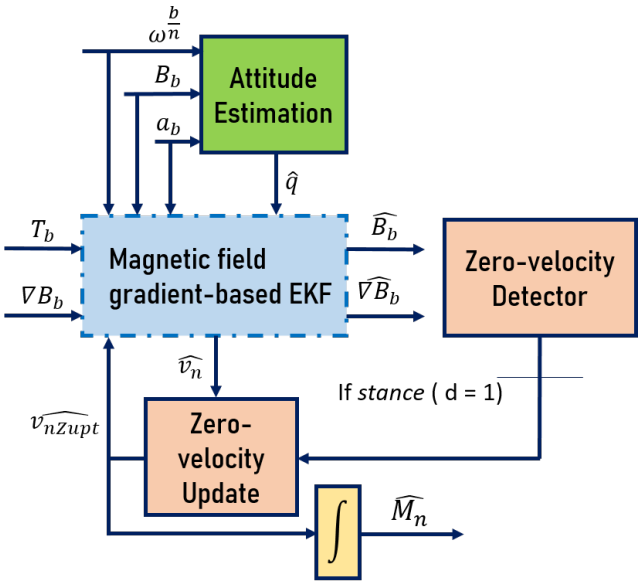

Figure 4. ZUPT-aided position estimation

with $T_s(a_b, \omega^{\frac{b}{n}})$, the test statistics of the detector and γ, the detection threshold.
The test statistics can have multiple forms depending on the chosen detector. In related works, different detectors have been evaluated [10] from the ones depending only on accelerometer data (such as Acceleration Moving Variance Detector and Acceleration Magnitude Detector), to those that are angular rate-based (Angular Rate Energy Detector), or even pressure measurements [32]. In this paper, the Stance Hypothesis Optimal Detector (SHOE) [33] is chosen, as it represents a combination between acceleration and angular rate-based detectors, and has proven to outperform other detectors in the literature for its robustness to changes in gait speed as well as its high positional accuracy. Concretely, SHOE computes $T_s(a_b, \omega^{\frac{b}{n}})$ in the following way,

$$T_s(a_b, \omega^{\frac{b}{n}}) = \frac{1}{W} \sum_{k=l}^{l+W-1} \left(\frac{1}{\sigma_a^2} ||a_{b,k} - g \frac{\bar{a}_{b,l}}{||\bar{a}_{b,l}||}||^2 + \frac{1}{\sigma_\omega^2} ||\omega_k{}^{\frac{b}{n}}||^2 \right) \tag{15}$$

where W is the window size (the number of sensor readings), σ_a^2, σ_ω^2 are the variances of the acceleration and angular rate measurements, $\bar{a}_{b,l}$ denotes the mean over W samples, and g is the gravity.

4.2. ZUPT

If the detector d has declared the stationary case (i.e. $d = 1$), $\widehat{v_n}$ should give a zero-velocity estimate. However, due to diverse errors, it most likely will not. This motivates the use of ZUPT, as it corrects these drifts, which greatly improves the velocity estimation, as it was shown in the literature. If $d = 1$ at time k, the actual value of inertial velocity is assumed to be known, and then its estimate $\widehat{v_n}$ is reset to zero. This is actually done inside the EKF, in a way where the velocity estimate $\widehat{v_n}$ is constantly corrected. In Fig. 4, the ZUPT-based velocity estimate is represented with $\widehat{v_{nZupt}}$. Consequently, by updating the velocity estimate, a better position estimation should be obtained after integrating $\widehat{v_{nZupt}}$ (yellow box in Fig. 4).

5. Simulations and results

In this section, the performance of the proposed magnetic field gradient-based EKF is displayed. The improvements on inertial velocity estimation are highlighted when ∇B_b is filtered. In the end, we examine the effect of such improvement on the position in a foot-mounted navigation framework aided by ZUPT.

5.1. Groundwork for simulations

One of the most common problems in pedestrian navigation, is the knowledge of ground truth, as it enables to compare proposed algorithms and contributions with references. In [22], authors simulate a trajectory (position and attitude), that is based on a real human walk pattern. A synthetic noiseless IMU data is provided. A set of signals from a spatially distributed magnetometers array is also considered (one signal is given by [22] and the others are simulated accordingly). The reader can refer to this website: https://lopsi.weebly.com/downloads.html, to download one of the proposed data sets corresponding to ground truth trajectories, and to have more details about the different chosen parameters. In this simulation, a closed 3-loop trajectory in rectangular path of $12 \times 7m$ is used to represent the ground truth. Then, an additive random zero-mean white Gaussian noise is added as detailed in Table 1.

Table 1. Standard deviations of considered noises from datasheet of MTi module (Xsens) [34]

	Noise standard deviation
Accelerometer $[ms^{-2}]$	**0.012**
Gyroscope $[rads^{-1}]$	**0.0087**
Magnetometers $[G]$	**0.03**

5.2. Main results

5.2.1. Attitude estimation results

To determine the body attitude in quaternion, Madgwick's gradient descent algorithm [25] is used, as it has been proven robust to magnetic disturbances. The constant $\beta = 0.008$ (divergence rate) is fixed through a trial and error scheme and by taking into account gyroscope measurements error. The estimated quaternion $\widehat{q}$ is used to calculate the rotation matrix $R(\widehat{q})$ through (1). This matrix is important in velocity estimation as it is used in the model in Fig. 3. The estimated quaternion is converted into Euler angles as shown in Fig. 5.

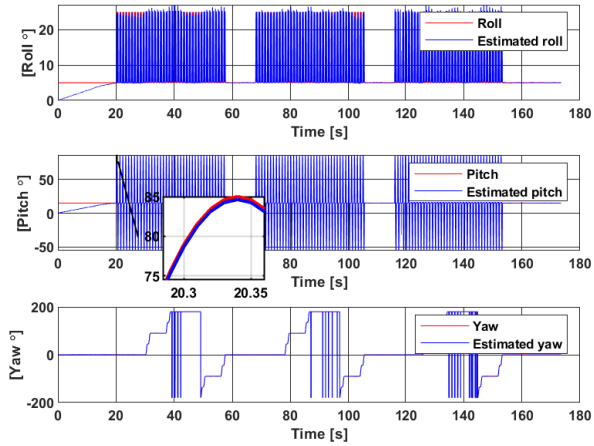

Figure 5. Euler angles estimation through Madgwick filter [25]

The estimated Euler angles converge in less than $20s$ despite initializing the EKF with values that are different from the true ones. Moreover, the filter is robust against the high standard deviation noise added to magnetic measurements. However, some jumps are seen on the *yaw* estimation when the

angle reaches 180°, which is explained by the fact that quaternion cannot represent a rotation exceeding 180° in any direction. This affects position reconstruction along the z-axis.

5.2.2. Magnetic field gradient-based EKF results

As proposed earlier in this paper, ∇B_b should be filtered from noise, in the purpose of better estimating the inertial velocity. Fig. 6 displays the estimation results for the first element α_{11} of ∇B_b. The estimated gradient (in blue dashed line) is close to the theoretical one (in red solid line) even though the initialization values are different from the ground-truth ones.

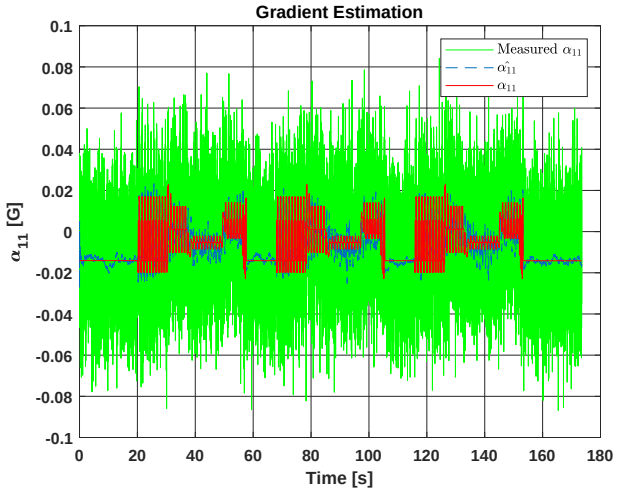

Figure 6. Estimation of the first element α_{11} of ∇B_b

Let $\eta_{\alpha_{11}}$ represent the noise of the first element α_{11} of ∇B_b. In Fig. 7, the Power Spectral Density (PSD) [35] of this noise is presented, before and after filtering ∇B_b with the proposed EKF. This metric represents the square of Fourier transformation module, divided by the spectral bandwidth. It basically describes how the power of a signal is distributed over frequency, which is an interesting criterion to evaluate the noise compensation.

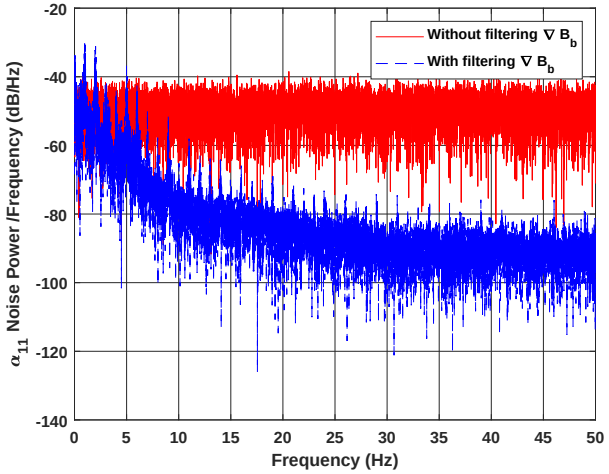

Figure 7. α_{11} noise PSD with and without filtering ∇B_b

Fig. 7 shows that in case ∇B_b is filtered (by adding (10) to (11)), the noise power of its elements (e.g. α_{11} in this case), represented in blue dashed line, is inferior than the one of when the filtering process is not applied (when ∇B_b is not in the state vector), represented in red solid line, and it decreases continuously along the frequency range. The mean of noise PSD error between both cases is

around $\approx -29.77\ dB$, which justifies the effectiveness of the proposed approach. Another way that is used to quantify noise in a signal is by computing the Signal to Noise Ratio (SNR) [35], which is the ratio of the power of true signal α_{11} to the power of its noise $\eta_{\alpha_{11}}$. The SNR of α_{11} increases from $SNR_{without} = -9.46\ dB$ when ∇B_b is not filtered, to $SNR_{with} = -0.42\ dB$, when it is done. This proves again that ∇B_b noise is greatly reduced with the proposed model and filter.
The advantage of this filtering process is also observed during the velocity estimation, as shown in Fig. 8, where the x axis component of the inertial velocity is plotted. The velocity estimate $\widehat{v_{nx}}$ (green solid line) given by the proposed approach is closer to the ground truth velocity (red solid line) than when ∇B_b is used as a noisy input (blue solid line).

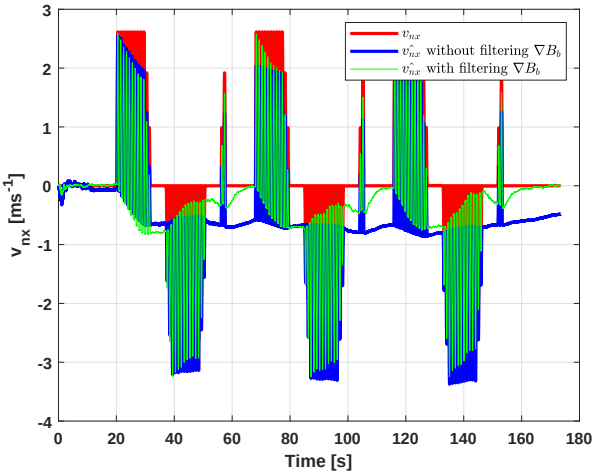

Figure 8. Estimation of v_{nx} with and without filtering ∇B_b

As indicated in Table 2, the RMSE between the estimated velocity $\widehat{v_n}$ and the true one v_n is 0.37 ms^{-1} for the case where the proposed approach is not applied, versus 0.27 ms^{-1} when it is done. This improvement is beneficial in some applications that require measuring the velocity with a certain precision. The performance of the magnetic field gradient-based EKF is also compared to the first work [24] and better results are shown in terms of velocity RMSE. This improvement is obtained thanks to the better tuning of the state and measurement noise covariance matrices of the proposed EKF. From Table 2, it can be seen that the main contribution of this work resides on the yellow colored line, where the smallest value of RMSE compared to the other approaches is observed.

Table 2. RMSE of the velocity estimation

	$v_n\ RMSE\ [ms^{-1}]$
Without filtering ∇B_b	**0.37**
With filtering ∇B_b in a primary EKF [24]	**0.29**
With filtering ∇B_b	**0.27**

5.2.3. Application: Extending to position estimation

One possible application that highlights the importance of the decrease on the velocity estimation error, is the position reconstruction through an integration of $\widehat{v_n}$ (without ZUPT). The impact can be seen by plotting the 2D representation of the estimated trajectory. A noticeable drift compensation is observed when ∇B_b is filtered. Indeed, the slightest improvement in velocity estimation can largely affect the reconstruction of trajectory, as less errors are generated, and thus less of their accumulation during the integration process. Table 3 presents the RMSE between the estimated position and the ground truth for the three studied approaches. As the case for velocity, the best results are achieved

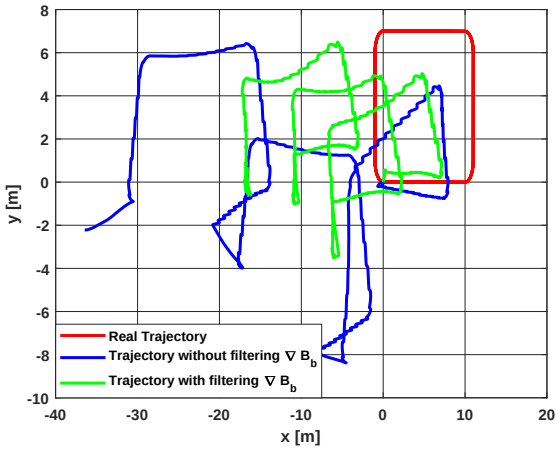

Figure 9. 2D trajectory reconstruction with and without filtering ∇B_b

when ∇B_b is filtered with the proposed EKF. This is clearly expected as the position is obtained from integrating the estimated velocity $\widehat{v_n}$.

Table 3. RMSE of the position estimation

	M_n $RMSE$ $[m]$
Without filtering ∇B_b	**31.60**
With filtering ∇B_b in a primary EKF [24]	**25.18**
With filtering ∇B_b	**20.88**

Now despite the previously mentioned contribution in inertial velocity estimation, the obtained error results are still considered high if position reconstruction needs to be done, which is observed in Table 3. In fact, whether its computed with or without the proposed model, $\widehat{v_n}$ still suffers from some errors, which are due to the different uncertainties considered in the simulation scenario, i.e. the approximations taken into account to extract the spatial derivatives (T_b for instance), the linearization process of the EKF, the tuning of the process and measurements covariances, etc. These errors lead to drifts if position needs to be reconstructed, which is seen in Fig. 9. Note also that a noise with a large standard deviation is applied on magnetometers measurements, in order to better highlight the contribution of filtering ∇B_b. Nevertheless, better velocity estimation results can be obtained in case the values of the different noises are lowered, which improves consequently the position reconstruction.

5.2.4. Zero-velocity update results

For the different reasons stated above, the proposed magnetic field gradient-based EKF is combined with ZUPT (the red blocks in Fig. 4), and the same comparisons are done on the position reconstruction as the ones in Fig. 9. The pertinence of this approach on the velocity estimation in the case of foot-mounted applications is discussed in Section 4. By correcting the velocity estimate $\widehat{v_n}$ with ZUPT, better position estimation results are obtained, and drifts on all 3-axis are almost entirely removed. In fact, Fig. 10 shows that even when adding ZUPT, the proposed approach (with filtering ∇B_b), still outperforms the case of when the filtering is not applied (use ∇B_b as a noisy input). Note that the starting and arrival points for the ground truth trajectory are the same (red dot). It is observed that the arrival point of the green plot is closer to the ground truth one than the blue plot, which highlights the contribution of filtering ∇B_b. It can also been seen from the points coordinates that the drift on the z axis is greatly reduced in the case of filtering ∇B_b. In Table 4, a comparison between position RMSEs is displayed when ZUPT is added, which shows how the latter is reduced when ∇B_b

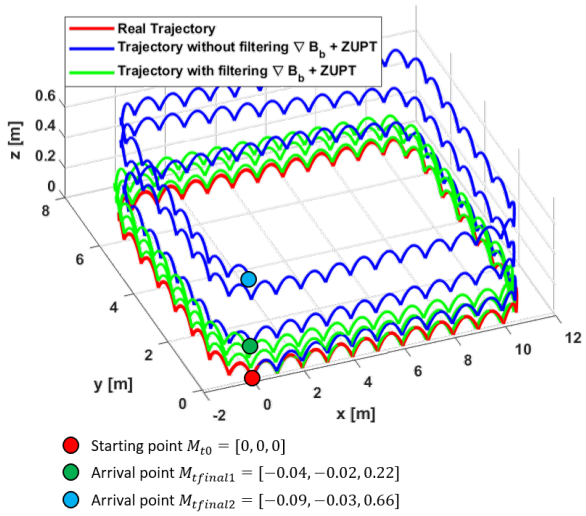

Figure 10. Trajectory reconstruction aided by ZUPT with and without filtering ∇B_b

is filtered. The obtained distance error with the proposed EKF after adding ZUPT also decreases from 1.22% of the total traveled distance to 0.41% with the proposed approach, which proves again the importance of filtering ∇B_b.

Table 4. Results of ZUPT-aided position estimation

	M_n *RMSE* $[m]$	*Distance error* $[\%]$
Without filtering ∇B_b + ZUPT	**0.26**	**1.22**
Filtering ∇B_b in a primary EKF+ZUPT	**0.14**	**0.88**
With filtering ∇B_b + ZUPT	**0.11**	**0.41**

6. Conclusion and future work

In this paper, the inertial velocity estimation was improved using a magnetic field gradient-based EKF. This was done by reducing noise from the magnetic field gradient, thanks to a newly introduced equation that better describes its dynamic. The proposed approach was then combined with ZUPT in order to estimate position in a foot-mounted application. Applying this approach on real experimental data is definitely the next step. Tuning the EKF covariance matrices with artificial intelligence-based approaches is also a topic that will be considered in future works.

Author Contributions: M.Z., currently a PhD student at GIPSA-Lab, has achieved this work with the collaboration of her supervisors, H.F., associate professor at the University Grenoble Alpes, and C.P., CNRS Senior Researcher. The conceptualization, methodology and programming of this work were conducted by M.Z., the investigation and analysis of the different results were elaborated with the help of H.F. and C.P. The original draft preparation was done by M.Z., followed by corrections and refinements from H.F. and C.P. All authors have read and agreed to the published version of the manuscript.

Acknowledgments: This work has been partially supported by MIAI@Grenoble Alpes, (ANR-19-P3IA-0003).

Conflicts of Interest: The authors declare no conflict of interest.

References

1. Draghici, I.; Vasilateanu, A.; Goga, N.; Pavaloiu, B.; Guta, L.; Mihailescu, M.N.; Boiangiu, C. Indoor positioning system for location based healthcare using trilateration with corrections. International Conference on Engineering, Technology and Innovation (ICE/ITMC); , 2017; pp. 169–172.

2. Van Haute, T.; De Poorter, E.; Crombez, P.; Lemic, F.; Handziski, V.; Wirstrom, N.; Wolisz, A.; Voigt, T.; Moerman, I. Performance analysis of multiple Indoor Positioning Systems in a healthcare environment. *International Journal of Health Geographics* **2016**, *15*, 7.
3. Ridolfi, M.; Vandermeeren, S.; Defraye, J.; Steendam, H.; Gerlo, J.; Clercq, D.; Hoebeke, J.; De Poorter, E. Experimental Evaluation of UWB Indoor Positioning for Sport Postures. *Sensors* **2018**, *18*, 168.
4. Rantakokko, J.; Rydell, J.; Strömbäck, P.; Händel, P.; Callmer, J.; Tornqvist, D.; Gustafsson, F.; Jobs, M.; Grudén, M. Accurate and reliable soldier and first responder indoor positioning: Multisensor systems and cooperative localization. *IEEE Wireless Communications* **2011**, *18*, 10–18.
5. Duan, Y.; Lam, K.; Lee, V.C.S.; Nie, W.; Liu, K.; Li, H.; Xue, C.J. Data Rate Fingerprinting: A WLAN-Based Indoor Positioning Technique for Passive Localization. *IEEE Sensors Journal* **2019**, *19*, 6517–6529.
6. Xu, H.; Wu, M.; Li, P.; Zhu, F.; Wang, R. An RFID Indoor Positioning Algorithm Based on Support Vector Regression. *Sensors* **2018**, *18*, 1504.
7. Martín-Gorostiza, E.; García-Garrido, M.-A.and Pizarro, D.; Salido-Monzú, D.; Torres, P. An Indoor Positioning Approach Based on Fusion of Cameras and Infrared Sensors. *Sensors* **2019**, *19*, 2519.
8. Michel, T.; Genevès, P.; Fourati, H.; Layaïda, N. Attitude estimation for indoor navigation and augmented reality with smartphones. *Pervasive and Mobile Computing* **2018**, *46*, 96–121.
9. Fourati, H. Heterogeneous data fusion algorithm for pedestrian navigation via foot-mounted inertial measurement unit and complementary filter. *IEEE Transactions on Instrumentation and Measurement* **2015**, *64*, 221–229.
10. Skog, I.; Nilsson, J.O.; Händel, P. Evaluation of zero-velocity detectors for foot-mounted inertial navigation systems. International Conference on Indoor Positioning and Indoor Navigation (IPIN); , 2010; pp. 1–6.
11. Fourati, H.; Manamanni, N.; Afilal, L.; Handrich, Y. A Nonlinear Filtering Approach for the Attitude and Dynamic Body Acceleration Estimation Based on Inertial and Magnetic Sensors: Bio-Logging Application. *IEEE Sensors Journal* **2011**, *11*, 233–244.
12. Gabaldon, J.; Turner, E.; Johnson-Roberson, M.; Barton, K.; Johnson, M.; Anderson, E.; Shorter, K. Integration, Calibration, and Experimental Verification of a Speed Sensor for Swimming Animals. *IEEE Sensors Journal* **2019**, *19*, 3616–3625.
13. Erdelić, M.; Carić, T.; Ivanjko, E.; Jelušić, N. Classification of Travel Modes Using Streaming GNSS Data. *Transportation Research Procedia* **2019**, *40*, 209–216.
14. Yang, X.; Stewart, K.; Tang, L.; Xie, Z.; Li, Q. A Review of GPS Trajectories Classification Based on Transportation Mode. *Sensors* **2018**, *18*, 3741.
15. Bachmann, E.R.; Yun, X.; Peterson, C.W. An investigation of the effects of magnetic variations on inertial/magnetic orientation sensors. International Conference on Robotics and Automation; , 2004; pp. 1115–1122.
16. Jackson, J. *Classical Electrodynamics*; Third Edition. John Wiley & Sons, Inc., 1998.
17. Skog, I.; Hendeby, G.; Gustafsson, F. Magnetic Odometry - A Model-Based Approach Using a Sensor Array. International Conference on Information Fusion (FUSION); , 2018; pp. 794–798.
18. Vissière, D.; Martin, A.; Petit, N. Using spatially distributed magnetometers to increase IMU-based velocity estimation in perturbed areas. Conference on Decision and Control; , 2007.
19. Vissière, D.; Martin, A.; Petit, N. Using magnetic disturbances to improve IMU-based position estimation. European Control Conference; , 2007; pp. 2853–2858.
20. Chesneau, C.I.; Hillion, M.; Hullo, J.F.; Thibault, G.; Prieur, C. Improving magneto-inertial attitude and position estimation by means of a magnetic heading observer. International Conference on Indoor Positioning and Indoor Navigation (IPIN); , 2017; pp. 1–8.
21. Dorveaux, E.; Boudot, T.; Hillion, M.; Petit, N. Combining inertial measurements and distributed magnetometry for motion estimation. American Control Conference; , 2011; pp. 4249–4256.
22. Zampella, F.J.; Jiménez, A.R.; Seco, F.; Prieto, J.C.; Guevara, J.I. Simulation of Foot-Mounted IMU Signals for the Evaluation of PDR Algorithms. International Conference on Indoor Positioning and Indoor Navigation (IPIN); , 2010; pp. 1–6.
23. Kuipers, J. *Quaternions and rotation sequences*; 1999.
24. Zmitri, M.; Fourati, H.; Prieur, C. Improving Inertial Velocity Estimation Through Magnetic Field Gradient-based Extended Kalman Filter. International Conference on Indoor Positioning and Indoor Navigation (IPIN); , 2019.

25. Madgwick, S.O.; Harrison, A.J.; Vaidyanathan, R. Estimation of IMU and MARG orientation using a gradient descent algorithm. International Conference on Rehabilitation Robotics; , 2011; pp. 1–7.
26. Süli, E. *Numerical Solution of Ordinary Differential Equations*; 2010.
27. Choukroun, D.; Bar-Itzhack, I.Y.; Oshman, Y. A Novel Quaternion Kalman Filter. *IEEE Transactions on Aerospace and Electronic Systems* **2006**, *24*, 174–190.
28. Renaudin, V.; Combettes, C. Magnetic, acceleration fields and gyroscope quaternion (MAGYQ)-based attitude estimation with smartphone sensors for indoor pedestrian navigation. *IEEE Transactions on Aerospace and Electronic Systems* **2014**, *14*, 22864–22890.
29. Mahony, R.; Hamel, T.; Pflimlin, J.M. Nonlinear complementary filters on the special orthogonal group. *IEEE Transactions on Automatic Control* **2008**, *53*, 1203–1218.
30. Wu, J.; Zhou, Z.; Fourati, H.; Li, R.; Liu, M. Generalized Linear Quaternion Complementary Filter for Attitude Estimation from Multi-Sensor Observations: An Optimization Approach. *IEEE Transactions on Automation Science and Engineering* **2019**, *16*, 1330–1343.
31. Martin, P.; Salaun, E. Design and implementation of a low-cost observer-based attitude and heading reference system. *Control Engineering Practice* **2010**, *18*, 712–722.
32. Ming, M.; Song, Q.; Gu, Y.; Li, Y.; Zhou, Z. An Adaptive Zero Velocity Detection Algorithm Based on Multi-Sensor Fusion for a Pedestrian Navigation System. *Sensors* **2018**, *18*, 3261.
33. Skog, I.; Händel, P.; Nilsson, J.O.; Rantakokko, J. Zero-Velocity Detection—An Algorithm Evaluation. *IEEE Transactions on Biomedical Engineering* **2010**, *57*, 2657–2666.
34. Xsens MTi Products. https://www.xsens.com/mti-products. Accessed: 2020-07-21.
35. Oppenheim, A.V.; Verghese, G.C. *Signals, Systems and Inference*; 2015.